https://doi.org/10.5194/esd-2019-42
Preprint. Discussion started: 5 August 2019
© Author(s) 2019. CC BY 4.0 License.

Earth System Dynamics Discussions
Open Access
EGU

Tropical and mid-latitude teleconnections interacting with the Indian summer monsoon rainfall: A Theory-Guided Causal Effect Network approach

Giorgia Di Capua[1,2], Marlene Kretschmer[1], Reik V. Donner[1,3], Bart van den Hurk[2,4], Ramesh Vellore[5], Raghavan Krishnan[5], and Dim Coumou[1,2]

[1]Potsdam Institute for Climate Impact Research, Potsdam, Germany
[2]VU University of Amsterdam, Institute for Environmental Studies, Amsterdam, Netherlands
[3]Magdeburg-Stendal University of Applied Sciences, Magdeburg, Germany
[4]Deltares, Delft, Netherlands
[5]Indian Institute for Tropical Meteorology, Pune, India

Correspondence to: Giorgia Di Capua (dicapua@pik-potsdam.de)

https://doi.org/10.5194/esd-2019-42
Preprint. Discussion started: 5 August 2019
© Author(s) 2019. CC BY 4.0 License.

Earth System Dynamics Discussions

Abstract.

The alternation of active and break phases in the Indian summer monsoon (ISM) rainfall at sub-seasonal timescales characterizes each ISM season. Tropical and mid-latitude drivers influence this sub-seasonal ISM variability. The circumglobal teleconnection observed in boreal summer drives sub-seasonal variability across the mid-latitudes and a two-way interaction between ISM and the circumglobal teleconnection pattern has been hypothesized. We use causal discovery algorithms to test the ISM-circumglobal teleconnection hypothesis in a causal framework. Our analysis shows a robust causal link from the circumglobal teleconnection pattern and the North Atlantic region to ISM rainfall. We estimate the normalized causal effect (CE) of this link to be about 0.2 (a one standard deviation shift in the circumglobal teleconnection causes a 0.2 standard deviation shift in the ISM rainfall one week later). In turn, the ISM rainfall influences back the circumglobal teleconnection pattern, however weakly. Moreover, we identify causal links that represent the internal dynamics of the ISM convective cell at weekly timescales: Periods with strong updraft lead to strong rainfall one week later, but the resulting increase in static stability suppresses convection again. In our analyses, this internal ISM dynamics has the strongest CE of 0.5. Tropical Madden-Julian Oscillation variability has a CE of 0.2-0.3. Our results show that the most of the ISM variability on weekly timescales is due to internal dynamics of convective cell, but both tropical and mid-latitude teleconnections have a substantial influence. Identifying these local and remote drivers paves the way for improved sub-seasonal forecasts.

1 Introduction

The Indian summer monsoon (ISM) is crucial for the Indian society, which receives 75% of its total annual rainfall during the summer months June through September (JJAS). The ISM rainfall variability at sub-seasonal time-scales is characterized by periods of enhanced and reduced rainfall activity over the monsoon-core region of central India. These periods are usually referred to as active (wet) and break (dry) phases respectively. Prolonged active and break spells in the ISM can lead to floods or droughts and consequently have severe socio-economic implications for the Indian subcontinent. A salient semi-permanent feature of the ISM is the “monsoon trough” (MT) which manifests as a low pressure zone extending from north-western India into the Gangetic plains and the Bay of Bengal (Rao, 1976; Krishnamurti and Sugi, 1987; Choudhury and Krishnan, 2011). The rainfall amount over the MT region is generally used to define dry and wet spells within the ISM season (Krishnan et al., 2000; Gadgil and Joseph, 2003). The position and strength of MT significantly influences the spatial distribution of monsoon precipitation and associated agricultural productivity on the Indian subcontinent, and the internal dynamics of the ISM circulation itself provides a first mechanism for sub-seasonal rainfall variability (Pathak et al., 2017).

The land-sea temperature difference and the mid-tropospheric thermal forcing over the Tibetan Plateau are the prime drivers for the monsoon circulation (Yanai and Wu, 2006). Ascending motions over the Indian subcontinent enhance the northward

https://doi.org/10.5194/esd-2019-42
Preprint. Discussion started: 5 August 2019
© Author(s) 2019. CC BY 4.0 License.

air flux from the ocean toward the land thereby bringing moisture from the ocean and fuelling rainfall. The latent heat released by strong convective rainfall is important for sustaining the ISM circulation (Levermann et al., 2009). However, it has two opposing effects: on the one hand, the latent heat release in the early stage of an active phase enhances ascending motions by heating the mid-to-lower troposphere (Levermann et al., 2009). On the other hand, latent heat release, that propagates upward and heats the upper layers of the air column, tends to increase the static stability and inhibits further ascending motions (Saha et al., 2012). Also, rainy weather and cloudy skies can have a cooling effect on the surface in support of suppressing convection (Krishnamurti and Bhalme, 1976). While this thermodynamic perspective is useful to understand the quasi-biweekly variations of the ISM elements locally, the spatio-temporal variations in the evolution of active and break phases over the Indian monsoon region are known to involve interactions between the wind anomalies and the northward propagation of the major rain band anomalies of the monsoon intraseasonal oscillation (Chattopadhyay et al., 2009; Shige et al., 2017; Wang et al., 2006). Krishnan et al. (2000) hypothesized that the triggering of Rossby waves by suppressed convection over the Bay of Bengal initiates ISM breaks through northwest propagation of high pressure anomalies from the central Bay of Bengal into northwest India. They noted that the initiation of suppressed convection and anticyclonic anomalies over the equatorial Indian Ocean and central Bay of Bengal occurred a week prior to the commencement of a monsoon break over India followed by the traversing of suppressed anomalies from the central Bay of Bengal to northwest India in about 2-3 days.

At sub-seasonal timescales, both tropical and mid-latitude drivers have been proposed to influence the active and break phases of the ISM rainfall. For example, the Madden-Julian Oscillation (MJO) which governs the sub-seasonal tropical climate variability operating at 30-90 day timescale represents an important tropical driver of the ISM sub-seasonal variability (Zhang, 2005). MJO consists of a transient region of strong convective motions and enhanced precipitation, which propagates eastward from the tropical Indian Ocean to the tropical western Pacific. Normally, only one MJO convective cell is present in these regions. The MJO influences the ISM system with enhanced convective rainfall activity during active MJO phases and negative rainfall anomalies during suppressed MJO phases (Anandh et al., 2018; Mishra et al., 2017; Pai et al., 2011).

Next to tropical drivers, mid-latitude circulation, the North Atlantic variability and mid-latitude wave trains have been proposed to modulate the occurrence of active and break phases of ISM (Ding and Wang, 2005, 2007; Kripalani et al., 1997). A circumglobal teleconnection pattern, characterized by a wave number 5 that encircles the northern hemisphere, has been associated with anomalous monthly rainfall and surface air temperature across the entire mid-latitude range (Ding and Wang, 2005). On the one hand, wave trains originating from the North Atlantic may influence the sub-seasonal variability of the ISM and modulate the intensity of the ISM rainfall (Ding and Wang, 2007; Krishnan et al., 2009). On the other hand, the diabatic heat sources in association with ISM convection might reinforce the circumglobal wave train propagating downstream (Ding and Wang, 2005). Another recurrent coupled pattern of sub-seasonal variability between mid-latitude circulation and the ISM is the wave train originating from the north-eastern North Atlantic and propagating with an arch-shape trajectory through the western Siberian Plains into central Asia (Ding and Wang, 2007). An important feature of this

https://doi.org/10.5194/esd-2019-42
Preprint. Discussion started: 5 August 2019
© Author(s) 2019. CC BY 4.0 License.


wave train is the 200 hPa central Asian High which may be able to trigger positive rainfall anomalies over the ISM region. This wave train generated in the North Atlantic region might also aid in modulating the alternating active and break conditions over central India (Ding and Wang, 2007; Krishnan et al., 2009; Saeed et al., 2011).

Plain correlation and composite analysis are commonly used to assess the relationship between two or more climate variables (Ding and Wang, 2005; Lau and Kim, 2011; Vellore et al., 2014). However, correlation alone cannot distinguish whether the detected relationships represent actual causal connections or are only spurious links, due to autocorrelation, indirect links or common drivers. Recently, causal discovery algorithms have been developed and subsequently applied to gain insights into the physical links of the climate system (Kretschmer et al., 2016; Runge et al., 2015a; Schleussner et al., 2014). One can use such tools to test whether hypothesized links or teleconnections are likely to represent true physical pathways or rather artefacts due to spurious correlations. A careful analysis in the context of the ISM thus starts from physical theory and, hence, requires domain knowledge of ISM dynamics. Using this so-called "theory-guided causal discovery analysis", we here study the two-way causal links connecting both tropical and mid-latitude regions with the ISM. First, we assess whether the connection between the ISM and the mid-latitude wave trains can be considered causal in one or both directions. Next, we quantify the relative causal effect of tropical, extra-tropical and internal drivers on the ISM.

2 Data and Methods

2.1 Data

We define the monsoon trough (MT) region as the region between 18°-25°N and 75°-88°E. We analyse weekly rainfall sums over the MT region from the CPC-NCEP (0.25°x0.25°) observational gridded global rainfall dataset over the period 1979-2016 (Chen et al., 2008) and from the Pai et al. (0.25°x0.25°) observational gridded Indian rainfall dataset over the period 1979-2017 (Pai et al., 2015). In the remainder of this paper, we will mainly focus on the results obtained for the latter data set, while those for the former are provided as parts of the Supplementary Material. Using data taken from the ERA Interim reanalysis (Dee et al., 2011) for the period 1979-2017, precursor regions are calculated from weekly averaged gridded (1.5°x1.5°) fields including outgoing longwave radiation at the top of the atmosphere (OLR), vertical velocity at 500 hPa (W) and geopotential height at 200 hPa (Z200). The NAO weekly index is obtained by averaging daily data from NOAA (available at ftp://ftp.cpc.ncep.noaa.gov/cwlinks/norm.daily.nao.index.b500101.current.ascii). To identify MJO phases, we use the OLR MJO Index (OMI) provided by NOAA (https://www.esrl.noaa.gov/psd/mjo/mjoindex/). This metric features the first and second principal components obtained by the empirical orthogonal function (EOF) analysis of OLR in the tropical belt (between 30°N and 30°S) filtered to remove influences outside the MJO time scale (30-90 days). OMI PC2 corresponds to the first principal component of the Real-Time Multivariate MJO index (RMM1), which is widely used in the literature (Kiladis et al., 2014; Pai et al., 2011; Wheeler and Hendon, 2004). All time series of MT rainfall, Z200 and all datasets analysed in this work are detrended and anomalies are calculated at weekly time-steps. Thus, both the climatological and seasonal cycle are

https://doi.org/10.5194/esd-2019-42
Preprint. Discussion started: 5 August 2019
© Author(s) 2019. CC BY 4.0 License.

Earth System Dynamics Discussions

removed. Since the interannual variability may affect the analysis, we follow the approach proposed by Ding and Wang (2007) and filter the data by removing from each JJAS season its seasonal average.

2.2 Causal effect networks

We apply Causal Effect Networks (CEN) and the Response-Guided Causal Precursors Detection (RG-CPD) tool, two recently developed applications of the so-called Peter and Clark – Momentary Conditional Independence (PC-MCI)algorithm (Runge et al., 2014; Spirtes et al., 2000). A CEN detects and visualizes the causal relationships among a set of univariate time series of variables (Kretschmer et al., 2016). The network is constructed using the PC-MCI algorithm, which is a causal discovery algorithm able to distinguish between spurious and true causal links for different time lags of interest (Runge, 2018). The term "causal" rests on several assumptions (Spirtes et al., 2000; Runge, 2018):It should be understood as *causal relative to the set of analysed precursors*, meaning that the identified causal links are valid in the selected set of actors. Adding additional actors may change the structure of the causal network. It is therefore crucial to combine CEN with theoretical domain knowledge (i.e. our "theory-guided causal discovery analysis" approach). Other important assumption are stationarity of time series and near-linear interactions between actors.

The PC-MCI algorithm is a two-step algorithm based on a modified version of the PC algorithm (Runge et al., 2014; Spirtes et al., 2000). In the first step, the PC-step, identifies the relevant conditions for each variable by iterative independence testing. The following MCI-step tests whether the link between two actors can be considered causal. The false discovery rate (FDR) approach, as described by Benjamini and Hochberg, is applied to correct for inflated p-values due to multiple significance testing (Benjamini and Hochberg, 1995; Benjamini and Yekutieli, 2001). Each step is further described below.

In a variable set P containing n univariate detrended anomaly time series (*actors*), the PC-step identifies the *causal parents* of each element in P, among all the remaining elements in P. First, the PC algorithm calculates plain correlations between each i^{th} actor in P and all the remaining elements at a certain time lag τ. Those actors that significantly correlate with the i^{th} actor form the set of its initial parents P_i^0 at lag τ. Then, partial correlations between the i^{th} actor and each element in P_i^0 are calculated, conditioning first on one condition. If x, y and z are elements in P, the partial correlation between x and y conditioned on z is calculated by first performing linear regressions of x on z and of y on z and then calculating the correlation between the residuals. If the resulting partial correlation between x and y is still significant at a certain significance threshold α, x and y are said to be *conditionally dependent* given variable z, i.e., the correlation between x and y cannot be (exclusively) explained by the influence of variable z. When the opposite happens, the link is spurious and therefore filtered out, and x and y are called *conditionally independent*. This process leads to a reduced set of parents P_i^1. In the next step, the process is repeated but conditioning on two conditions, leading to a second set of parents P_i^2. The algorithm converges when the number of causal parents contained in P_i^n is equal or greater than the number of conditions needed to calculate the next partial correlation. At the end of the PC-step, each element in P has its own set of parents, which then enters the MCI-step. In the MCI-step, the partial correlation between an actor and its set of parents is calculated again but conditioned simultaneously on both the set of

https://doi.org/10.5194/esd-2019-42
Preprint. Discussion started: 5 August 2019
© Author(s) 2019. CC BY 4.0 License.

Earth System Dynamics Discussions

parents of the i^{th} actor and the sets of parents of each of the parents of the i^{th} actor. Those parents that pass the MCI test will then form the final set of parents for the i^{th} actor (Runge et al., 2017). A numerical example of these steps is given in the SI.

The causal links detected via the PC-MCI algorithm are visualized in terms of a causal effect network (CEN). Each CEN is composed by circles, representing the various actors, and by arrows, with the colour indicating the strength and the arrow the direction of the detected causal links. The strength is expressed by its associated path coefficient, defined as following Runge et al (2015a), as the "expected change in X^j (in units of its standard deviation [s.d] and relative to the unperturbed regime) at time t if X^i was perturbed at time $t-\tau$ by a one s.d. delta peak". To give an example, a path coefficient of 0.5 means that a change in the causal parent of 1 s.d. corresponds to a change in 0.5 s.d. in the response variable. Here, due to the fact that only lags at τ=1 are accounted for, the path coefficients also correspond to the total causal effect (CE). The path coefficient of each variable on itself is here referred to as the autocorrelation path coefficient. This should not be confused with the usual definition of the lag-1 autocorrelation coefficient. The autocorrelation path coefficient is the same as the path coefficient, where $i = j$ and it represents the causal influence of an actor on itself.

2.3 Response-guided causal precursor detection

RG-CPD identifies the causal precursors of a response variable based on multivariate gridded observational data (Kretschmer et al., 2017). It combines a response-guided detection step (Bello et al., 2015) with the PC-MCI causal discovery step (Runge et al., 2014; 2015a; 2015b; Spirtes et al., 2000). Without requiring an a priori definition of the possible precursors, RG-CPD searches for correlated precursor regions of a variable of interest (i.e. the *response variable*) in multivariate gridded data and then detects causal precursors by filtering out spurious links due to common drivers, autocorrelation effects or indirect links. Using correlation maps, an initial set of precursors is identified in relevant meteorological fields by finding regions in which the recorded variability precedes changes in the response variable at some lead time. Adjacent grid points with a significant correlation of the same sign at a level of α=0.05 are spatially averaged to create single one-dimensional time series, called *precursor region* (Willink et al., 2017). Correlation values are calculated with a two-sided *p*-value for a hypothesis test whose null hypothesis is that there is no correlation, using the Wald Test with a *t*-distribution of the test statistic. All *p*-values are corrected using the Benjamini and Hochberg FDR correction to address the variance inflation due to serial correlations (Benjamini and Hochberg, 1995; Benjamini and Yekutieli, 2001). In the second step, PC-MCI identifies the set of *causal precursors* for the response variable. The results present those precursor regions on a global map that are identified to be causally linked with the response variable (MT rainfall).

https://doi.org/10.5194/esd-2019-42
Preprint. Discussion started: 5 August 2019
© Author(s) 2019. CC BY 4.0 License.

Earth System Dynamics Discussions
Open Access
EGU

3 Results

3.1 Causal testing of the two-way ISM-circumglobal teleconnection mechanism

First, we assess whether the two-way interaction between the circumglobal wave train (that characterizes the boreal summer circulation) and the MT rainfall, as hypothesized by Ding & Wang (2005, hereafter DW2005), is reproduced using our CEN
185 analysis. We will refer to this theory as the monsoon-circumglobal teleconnection mechanism. We also analyse the influence of the North Atlantic on the MT rainfall, as hypothesized by Ding & Wang (2007, hereafter DW2007).

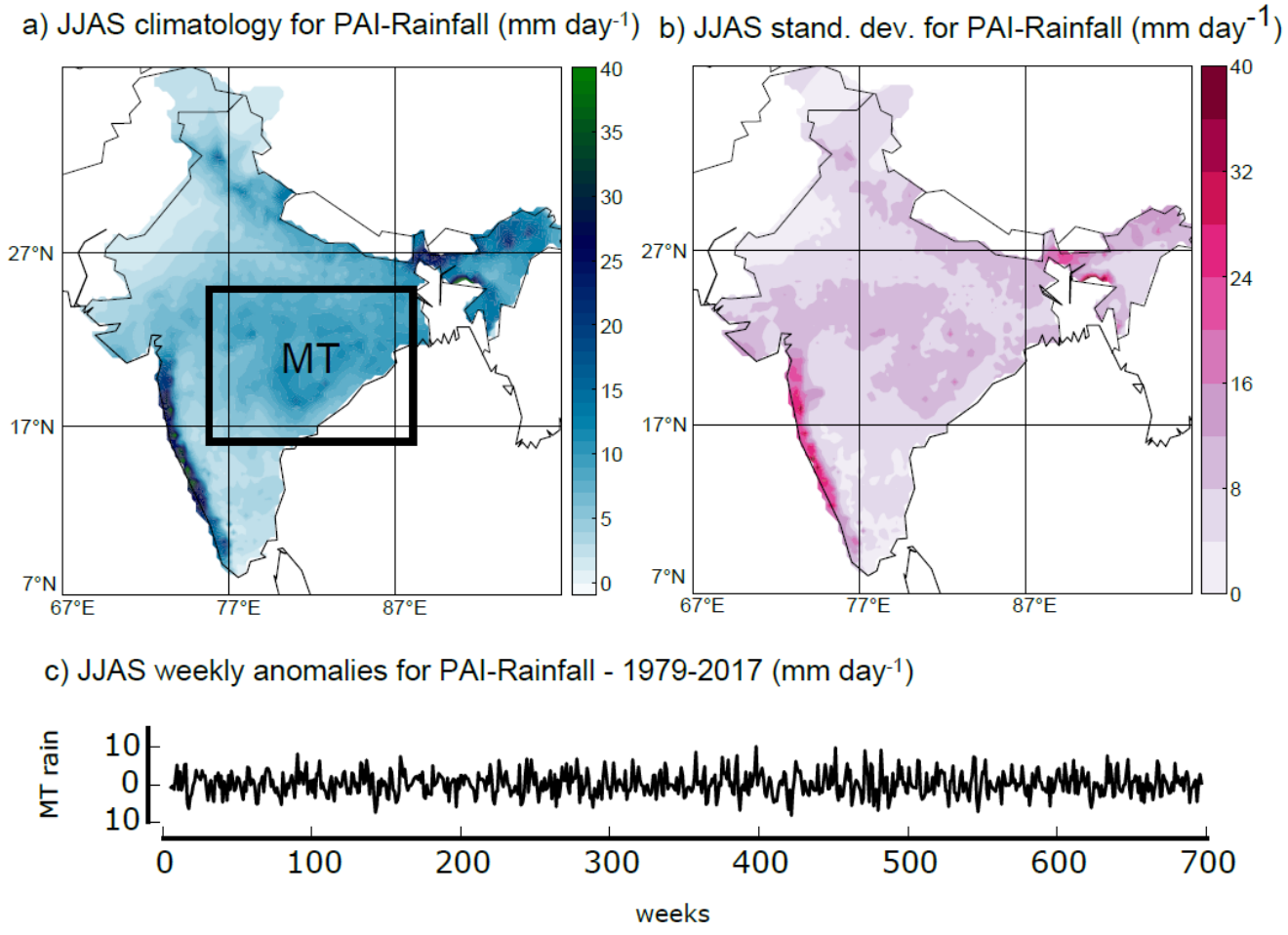

Figure 1. Rainfall climatology over India. Panel (a): JJAS rainfall climatology over the 1979-2017 period from the Pai et al. dataset. The black box identifies the MT region. Panel (b): standard deviation (s.d.) of weekly JJAS rainfall over the 1979-2017 period from the Pai et
190 al. dataset. Panel (c): time series of weekly MT JJAS rainfall over the period 1979-2017; each year contains 18 weeks, with the first week starting on the 27th of May.

https://doi.org/10.5194/esd-2019-42
Preprint. Discussion started: 5 August 2019
© Author(s) 2019. CC BY 4.0 License.

Earth System Dynamics Discussions

Figures 1a,b show the JJAS climatology and the s.d. of weekly ISM rainfall from the Pai et al. dataset for the period 1979-
195 2017. We average the rainfall over the MT region and identify a univariate time series, which represents the weekly variation of the ISM during JJAS over the MT region (Fig. 1c). This time series contains 18 weeks for each of the 39 analysed years, each year starting on the 27th of May. The analysis of the MT rainfall starts on the 3rd week (10th of June) for a total of 16 7-day time slots per year. The first two time slots allow detecting lagged relationships, and the PC-MCI algorithm requires to add twice the maximum time lag explored (here a maximum lag of 1 week is chosen). Thus, information from the previous
200 year does not interfere with the following year. The weekly time scale is considered to represent the relevant interaction between ISM rainfall and Northern Hemisphere atmospheric circulation at a sub-seasonal timescale (Ding and Wang, 2007; Krishnamurti and Bhalme, 1976; Vellore et al., 2014).

https://doi.org/10.5194/esd-2019-42
Preprint. Discussion started: 5 August 2019
© Author(s) 2019. CC BY 4.0 License.

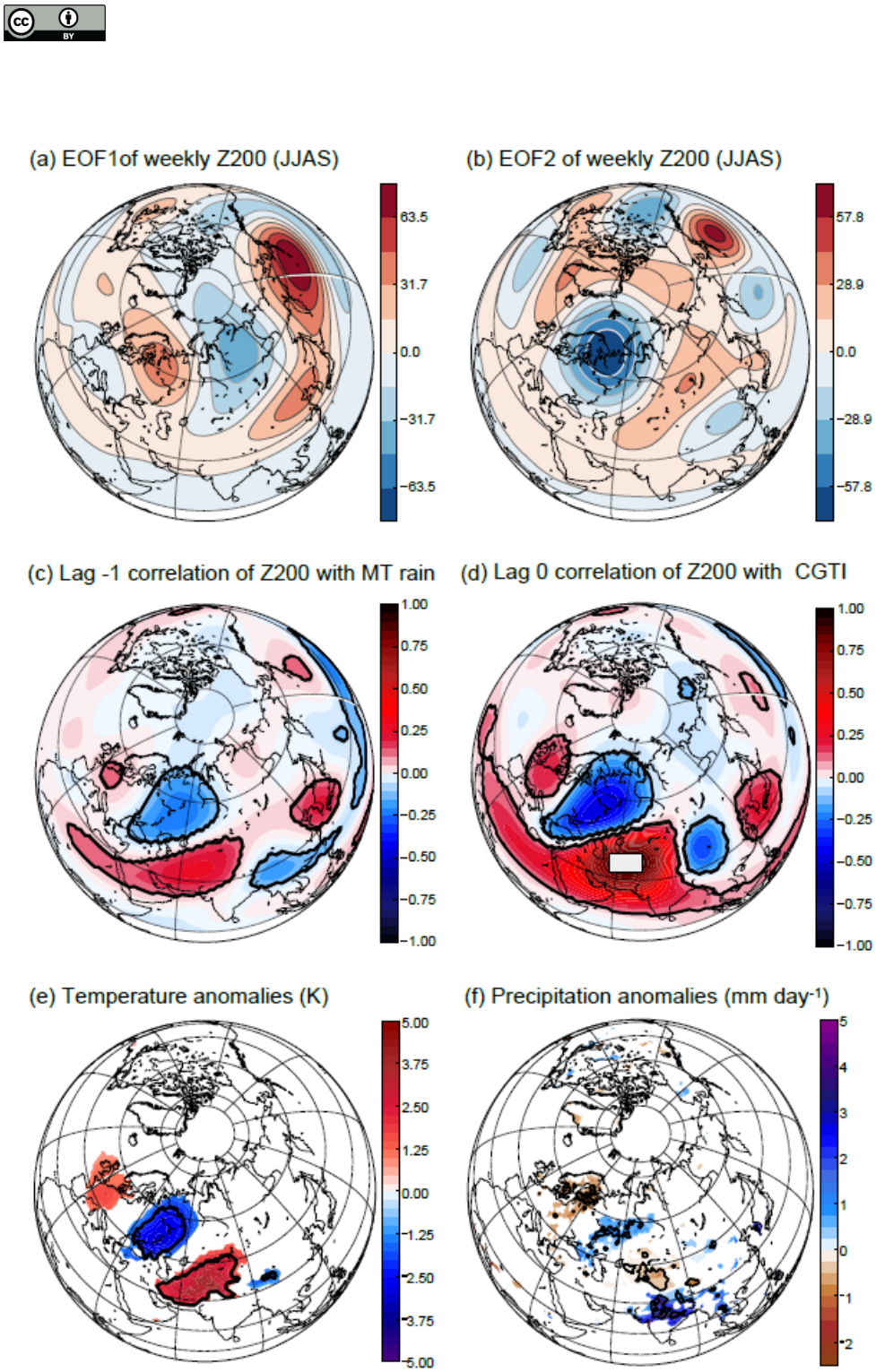

Figure 2. Mid-latitude variability associated with the ISM. Panels (a) and (b): EOF1 and EOF2 for the JJAS weekly Z200 field in the northern mid-latitudes for the period 1979-2017. Panel (c): correlation between weekly MT rainfall and Z200 (lag = -1 week). Panel (d): the CGTI region (white box) and the correlation between CGTI and Z200 (lag = 0), which forms the circumglobal teleconnection pattern. In panels (c) and (d), correlation coefficients and anomalies with a *p*-value of $p < 0.05$ (accounting for the effect of serial correlations) are

https://doi.org/10.5194/esd-2019-42
Preprint. Discussion started: 5 August 2019
© Author(s) 2019. CC BY 4.0 License.

Earth System Dynamics Discussions

shown by black contours. Panel (e): mean temperature anomalies over the Northern Hemisphere during weeks with CGTI > 1 $CGTI_{std}$ minus weeks with CGTI < -1 $CGTI_{std}$. Panel (f): as panel (e) but for rainfall anomalies from the CPC-NCEP dataset (as rainfall data for the Pai dataset are available over India only) for the period 1979-2017. In panels (e) and (f), anomalies with a *p*-value of $p < 0.05$ (accounting for the effect of serial correlations) are shown by black contours, while grid points which are found significant only with non-corrected *p*-values are shaded.

To analyse the major mode of Z200 variability in the Northern Hemisphere mid-latitudes, following DW2005, we calculate the first and second empirical orthogonal functions (EOFs) of weekly averaged Z200 fields over the Northern Hemisphere (0°-90°N) for the summer months coinciding with the ISM season (June to September, weeks 21 to 38). Figures 2a,b show the first and second EOFs. EOF1 represents the dominant component of sub-seasonal variability of the Z200 field, and qualitatively resembles the s.d. of Z200 (see Fig. S1 in the SI). EOF2 represents the second dominant pattern of sub-seasonal variability of the Z200 field. However, EOF1 and EOF2 explain respectively only 6.4% and 5.9% of the sub-seasonal variability, i.e. after removing mean annual cycle and interannual variability. The first 5 EOFs explain together 27.9% of the total variability. These low values are not surprising if we consider that the mean annual cycle and interannual variability have been removed, thus leaving only the disturbances from the year-specific mean state. We apply a test for pronounced separation of EOFs following North et al, (1982). This test is based on the eigenvalues of the EOF analysis and provides a rule of thumb to determine whether two EOFs are degenerate, i.e. “indistinguishable between their uncertainties” (for further details see North et al. 1982 and Hannachi et al. 2007). The North test shows that the first three EOFs are not well separated mutually, while EOF1 and EOF2 are well separated from EOF4 and EOF5 (see SI, Fig. S2). Similarly, DW2007 also found a twin EOF mode in their study, however their work focuses on the Eurasian sector only.

DW2005 define the ISM-circumglobal teleconnection mechanism at interannual and monthly time scale, DW2007 uses daily data (after removing the interannual variability) to analyse the influence of the Eurasian wave train initiated from the North Atlantic on the north-central Indian rainfall. Thus, first we need to show that the definition of the circumglobal-teleconnection pattern as in DW2005, also applies meaningfully at weekly timescales, with the interannual variability is filtered out. Figure 2c shows the spatial correlation structure of MT rainfall with the variability of Z200 in the Northern Hemisphere at weekly timescale with Z200 leading the MT rainfall by one week (lag = -1). Following DW2005, we define a circumglobal teleconnection index (CGTI) as the weekly-mean Z200 spatially averaged over the region 35°-40°N, 60°-70°E (white box in Fig. 2d). The contemporaneous (lag=0) spatial correlation structure between the CGTI and Z200, i.e. the circumglobal teleconnection pattern, is shown in Fig. 2d. A large region of strong positive correlation surrounds the Caspian Sea, while downstream, i.e. moving from west to east following the mid-latitude westerlies, a circumglobal wave train is shown with 4 positive centres of action positioned over east Asia, the North Pacific, North America and western Europe. Despite different temporal averaging, using different datasets and the fact that we remove the interannual variability, our results with 5 centres of positive correlation strongly resemble the circumglobal teleconnection pattern described by DW2005, in terms of sign and the geographical position of its centres of action. Thus, we conclude that the circumgobal teleconnection patter defined by the CGTI region manifests also at weekly time scale. Moreover, the wave pattern shown over Eurasia in Fig. 2c and 2d also

https://doi.org/10.5194/esd-2019-42
Preprint. Discussion started: 5 August 2019
© Author(s) 2019. CC BY 4.0 License.

Earth System Dynamics Discussions

resembles the wave pattern identified by DW2007. Thus, this resemblance represents the first hint that the circumglobal teleconnection pattern and the Eurasian wave train analysed by DW2007 share common elements, and llink the North Atlantic variavility to the ISM region. In both Fig. 2c and 2d correlation values with corrected *p*-values $p < 0.05$ are highlighted with black contours.

The circumglobal teleconnection pattern (Fig. 2d) shows a close to zero and non-significant spatial correlation with the EOF1 pattern. The spatial correlation of EOF2 (Fig. 2b) with the circumglobal teleconnection pattern (Fig. 2d) at a global scale is $r = 0.32 \pm 0.01$, and the spatial correlation with the circumglobal teleconnection pattern increases when limited to the Eurasian sector only ($r = 0.46 \pm 0.02$). Contrarily, the spatial correlation with EOF1 and the circumglobal teleconnection is also low when only the Eurasian sector is taken into account ($r = 0.05 \pm 0.03$). When EOFs are calculated only on the Eurasian sector (0°-90°N – 0°-150°E), the order of the first and second EOFs is reversed, but the spatial patterns are very similar: $EOF1_{Eurasia}$ is strongly spatially correlated with EOF2 ($r = 0.93 \pm 0.01$) and with the circumglobal teleconnection pattern ($r = 0.44 \pm 0.02$; see SI, Fig. S3). Thus, the choice of the region to calculate the EOFs does not strongly affect the results. Moreover, since we are interested in the two-way effects of the entire mid-latitude circulation and the MT rainfall, we decided to use the EOFs defined over the entire Northern Hemisphere (as shown in Figs. 2a,b).

The time series for the principal component of EOF2 also significantly correlates with the CGTI time series ($r = 0.26 \pm 0.07$) while the correlation for the first principal component is low and not significant ($r = -0.01 \pm 0.08$). The circumglobal teleconnection pattern also strongly resembles the correlation structure between MT rainfall and Z200 at lag -1 (Fig. 2c) with a spatial correlation of 0.69 ± 0.01. These findings are consistent with those of DW2005, and thus illustrate a likely interaction between MT rainfall and Z200 variability.

Temperature and precipitation anonalies during weeks with strong CGTI also exhibit a clear wave train pattern originating from Western Europe. We calculate 2m-temperature and precipitation anomalies of the composite of weeks with CGTI > 1 $CGTI_{std}$ minus composites of weeks with CGTI < -1 $CGTI_{std}$ (where $CGTI_{std}$ is the s.d. of the CGTI index). Figures 2e,f present the corresponding 2m-temperature and precipitation anomalies from the Pai et al. dataset, respectively, showing anomalies with *p*-values $p < 0.05$ shaded and highlighting anomalies that have corrected *p*-values $p < 0.05$ by black contours. In both variables, a wave train from Western Europe to India via European Russia is detected. Wet and cold anomalies appear over central India and European Russia, while warm and dry anomalies are found over Western Europe and east of the Caspian Sea. Warm and dry anomalies appear together, however precipitation anomalies show a slight eastward shift with respect to temperature anomalies. Precipitation anomalies are weaker than those found for 2m-temperature, however a clearly defined wave pattern appears over the Eurasian sector.

https://doi.org/10.5194/esd-2019-42
Preprint. Discussion started: 5 August 2019
© Author(s) 2019. CC BY 4.0 License.

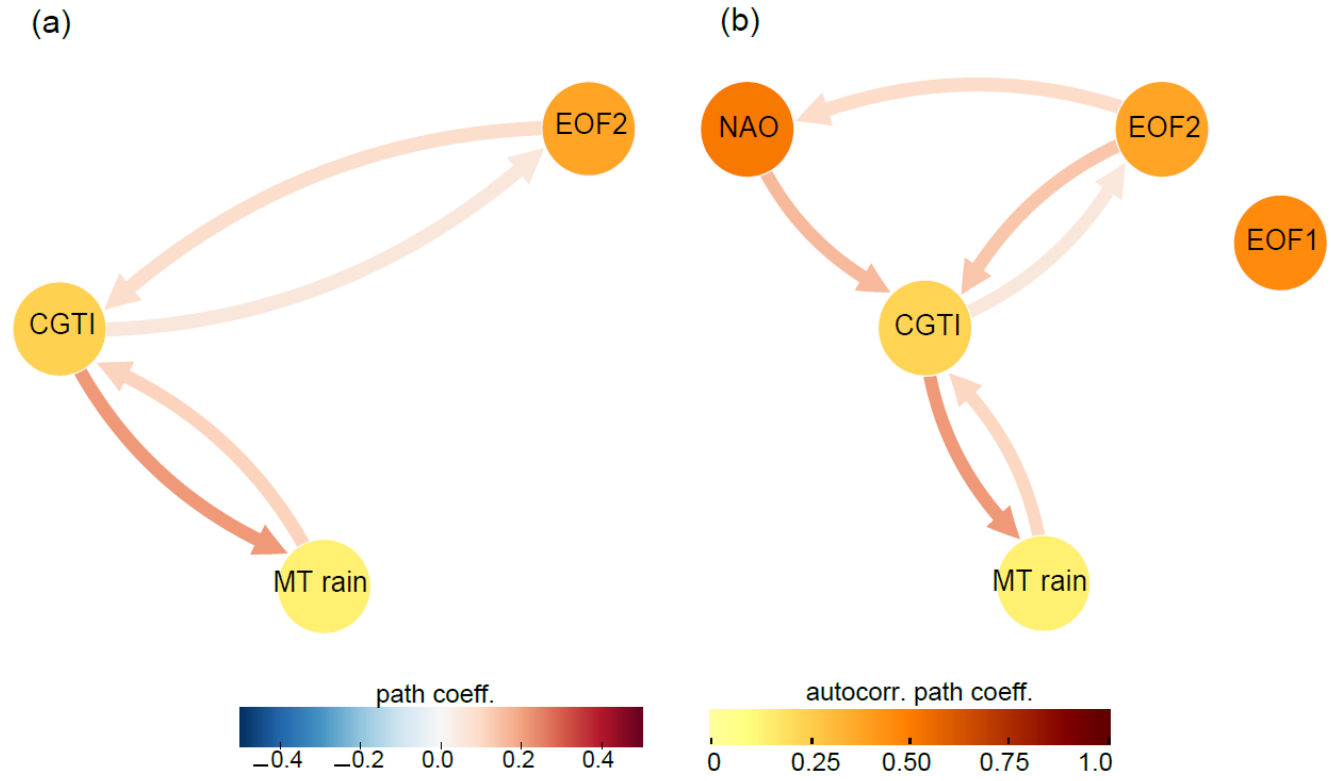

Figure 3. Causal mid-latitude interactions with the ISM. Panel (a): Causal Effect Network (CEN) built with CGTI, the PC of EOF2 and MT rainfall for the period 1979-2017. Panel (b): Same as panel (a) but with the addition of the PC of EOF1 and NAO. The strength of the causal links expressed by the standardized regression path coefficients and autocorrelation path coefficients are shown. All links have a lag of 1 week. See the main text for discussion.

Based on the DW2005 hypothesis, we build a CEN with CGTI, MT rainfall and the principal component of EOF2 (Fig. 3a). This CEN depicts a positive two-way connection both between CGTI and MT rainfall and between CGTI and EOF2. This implies that anomalously high CGTI values (with relatively high Z200 east of the Caspian Sea) enhance MT rainfall at a 1-week lag, while lower CGTI values have the opposite effect. The link directed from MT rainfall to CGTI illustrates a reverse influence, creating a positive feedback between CGTI and MT rainfall, consistent with DW2005. The strength of the causal link between the CGTI and MT rainfall is expressed by the path coefficients (see Methods section).

The causal link strength of the CGTI acting on the MT rainfall is $\beta_{CGTI \rightarrow MT}$ ~0.2 (meaning that a change of 1 s.d. in CGTI leads to a change in 0.2 s.d in MT rainfall, while the reverse link is weaker ($\beta_{MT \rightarrow CGTI}$~0.1) but still significant. EOF2 shows a two-way link with the CGTI. The links between EOF2 and CGTI support the DW2005 hypothesis that wave trains in the mid-latitudes (represented by EOF2) affect the MT rainfall via the CGTI.

https://doi.org/10.5194/esd-2019-42
Preprint. Discussion started: 5 August 2019
© Author(s) 2019. CC BY 4.0 License.

Earth System Dynamics Discussions

To assess whether the North Atlantic variability affects the MT rainfall (as hypothesized by DW2007), we add the NAO index to our original CEN. In order to check whether the first mode of variability in the Northern Hemisphere may also play a role in shaping MT rainfall variability, we additionally include EOF1. Figure 3b shows the resulting CEN: the causal links identified in the previous CEN (Fig. 3a) remain unaltered, and two additional positive links from NAO to CGTI and from the EOF2 to the NAO emerge. A positive NAO phase will strengthen the CGTI at 1-week lag ($\beta_{NAO\rightarrow CGTI}$~0.2) with a reverse influence from EOF2 on NAO ($\beta_{EOF2\rightarrow NAO}$~0.1), though weaker. EOF1 does not show a causal connection with CGTI or with any other actor. This CEN unveils both an influence of the mid-latitude atmospheric dynamics (EOF2) and North Atlantic variability (NAO) on MT rainfall and back, with the CGTI acting as a gateway, thus supporting both the DW2005 and DW2007 hypotheses. Substituting EOF2 with its corresponding EOF calculated over the Eurasian sector, $EOF1_{Eurasia}$, shows consistent results (see SI, Fig. S4).

3.2 Regional extratropical features affecting the Indian summer monsoon

The EOF-based CEN analysis depicts the total hemispheric response of Z200 without differentiating among the influences of different geographical regions. To detect influential regions, we next apply RG-CPD to search for causal precursors of both the CGTI and MT rainfall at 1-week lead time in weekly OLR and Z200 fields. In the tropical belt, OLR is often used as a proxy of rainfall and convective activity due to its relation with the temperature at the top of the clouds. Deep convection is characterized by high altitude cloud tops and low emission temperatures (and thus low OLR values), while at clear sky conditions, the emission temperature of the land surface is higher and leads to larger OLR values (Krishnan et al., 2000).
Figure 4 summarizes our corresponding findings. The right column (Fig. 4) shows the MT region and represents lag 0. Moving towards the left, the second column shows the correlation maps (top) and causal precursors (bottom) of the MT rainfall identified at 1-week lead time in Z200 (Fig. 4c). Causal precursors describe an arch-shaped wave train from Western Europe to India. The wave train features one low-pressure region (L1 over European Russia) and two high-pressure regions (the CGTI and H1 over Western Europe). The leftmost column in Fig. 4 shows the correlation maps (top) and causal precursors (bottom) of the CGTI identified in the Z200 (Fig. 4a) and OLR (Fig. 4b) fields at 1-week lead time with respect to the CGTI (2-week lead time with respect to the MT rainfall). Again, both Z200 and OLR correlation maps show an arch-shaped wave pattern emanating from the North Atlantic and propagating towards the Caspian Sea via European Russia. The associated Z200 causal precursors for the CGTI clearly depict this mid-latitude wave train both in Z200 and OLR (Figs. 4a,b). In the Z200 field (Fig. 4a), the wave train features two lows (L1 over European Russia and L2 over the eastern North Atlantic) and two highs (the CGTI and H1 over Western Europe). OLR causal precursors (Fig. 4b) depict only the L1 and H1 components of the wave, as the correlation over L2 is not significant. Moreover, the prominent influence of the tropical belt on the CGTI is also detected (OLR1, Fig. 4b). This result further supports the hypothesis that a wave train coming from the mid-latitudes influences the ISM circulation system via the CGTI region as already shown in Fig. 2, while strong temperature and precipitation anomalies shown in Figs. 2e,f coincide markedly with the regions H1, L1 and CGTI identified in Figs. 4a,c. figure 4a shows a North

https://doi.org/10.5194/esd-2019-42
Preprint. Discussion started: 5 August 2019
© Author(s) 2019. CC BY 4.0 License.

Earth System Dynamics
Discussions
Open Access
EGU

Atlantic pattern that resembles a negative NAO, whereas Fig. 3b indicated a positive causal link from NAO on CGTI. This seaming mismatch is explained by the difference in pressure level and lead-time with a more positive NAO pattern at lag -2 (see SI, Fig. S5).

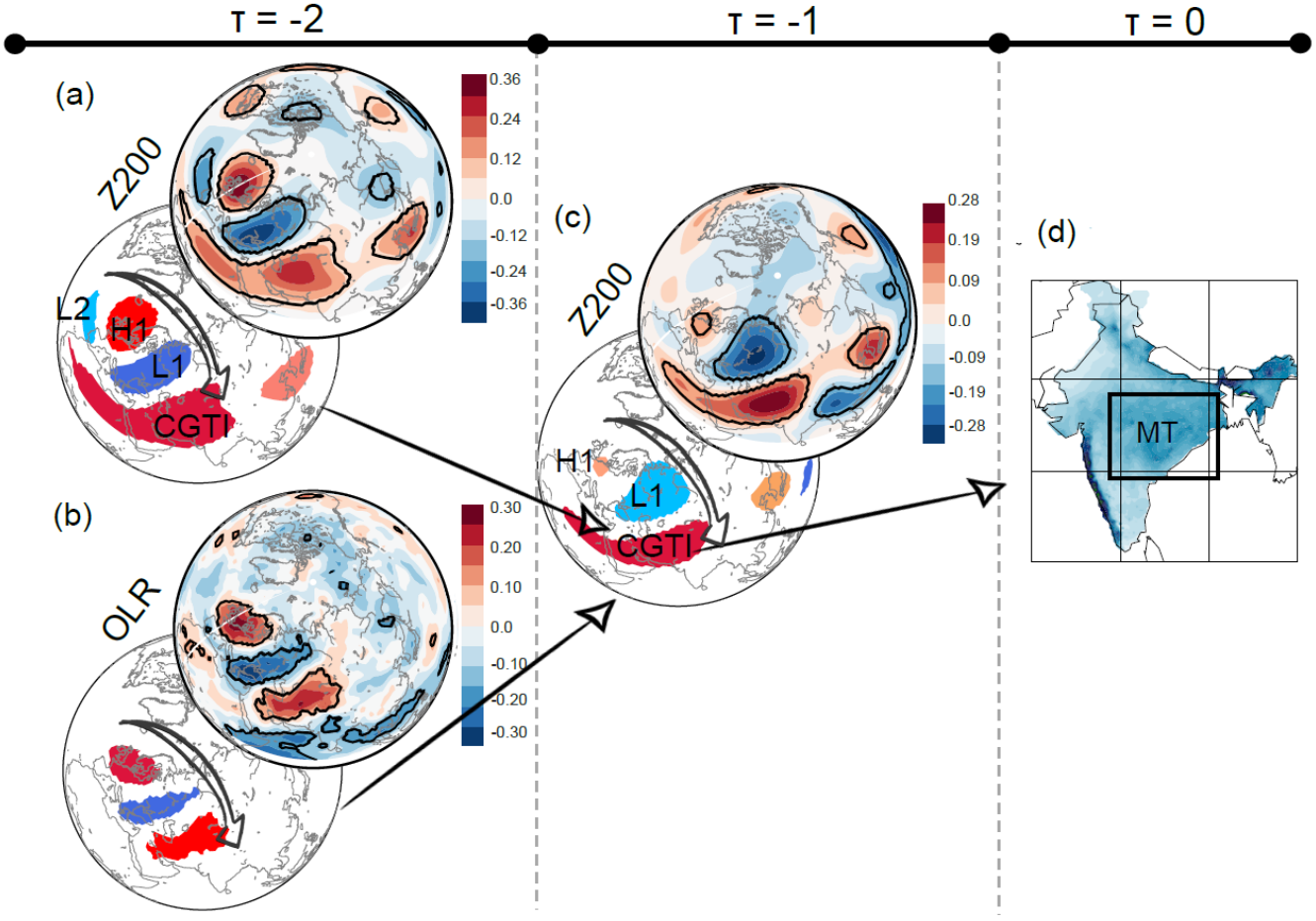

Figure 4. Mid-latitude causal precursors of ISM. Panel (a): correlation of CGTI with Z200 at 1-week lead time (top), and the causal precursors of CGTI identified via RG-CPD (bottom) for the period 1979-2017. Panel (b): as for panel (a) but for OLR fields. Panel (c): correlation map for weekly MT rainfall and Z200 field at 1-week lead time (top) and the causal precursors identified via RG-CPD (bottom). Panel (d): ISM rainfall over the MT region from the Pai et al. dataset (reproduced from Fig. 1a).

The CEN built with MT rainfall, CGTI and the upstream part of the mid-latitude wave train, i.e. L1 and H1, is shown in Fig. 5. The causal links between the CGTI and the MT rainfall remain unaltered (see Fig. 3), with the CGTI mediating the connection between the mid-latitude wave (represented by H1 and L1) and the MT rainfall. Further, the obtained CEN can be interpreted as a wave train that propagates eastward from the east Atlantic towards the Indian monsoon region, as postulated by DW2007. Let us focus on the connections between H1 and L1. If H1 increases, then L1 decreases at 1-week lag. The

https://doi.org/10.5194/esd-2019-42
Preprint. Discussion started: 5 August 2019
© Author(s) 2019. CC BY 4.0 License.

Earth System Dynamics Discussions
Open Access
EGU

backward link is positive: thus, if L1 increases H1 also increases at 1-week lag. This dampening loop is easiest explained by an eastward propagating wave. To illustrate this, we design a simple experiment using synthetic time series representing a simple cosine-wave propagating eastward with added noise sampled at two locations. We estimate the wavelength, wave speed and amplitude based on the observed properties of H1 and L1 (see SI, Fig. S7). The CEN resulting from these time series is equivalent to that of H1 and L1 in Fig. 5. With a negative forward link and a positive backward link. Physically, this can be understood in that a traveling wave amplifies in the forward direction, but at the same time dampens in the backward direction.

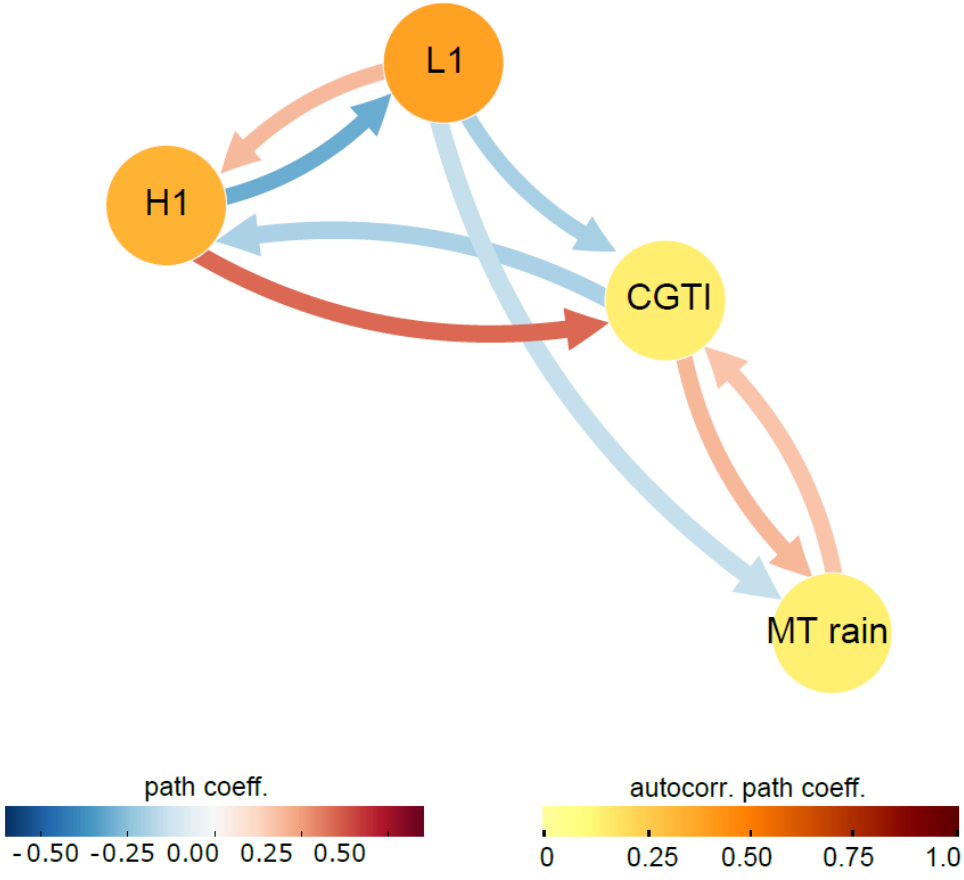

Figure 5. Mid-latitude wave train. CEN built with the MT rainfall, CGTI, L1 and H1 (as identified in Fig. 4a) for the period 1979-2017. The strength of causal links expressed by the standardized regression path coefficients and autocorrelation path coefficients are shown. All links have a lag of 1 week. See the main text for discussion.

https://doi.org/10.5194/esd-2019-42
Preprint. Discussion started: 5 August 2019
© Author(s) 2019. CC BY 4.0 License.

Earth System Dynamics Discussions

3.3 Internal feedbacks in the monsoon circulation

Next, we perform a similar analysis using fields of vertical wind velocities (W) and OLR to capture the internal feedbacks and dynamics of the ISM convective updraft. Their correlation maps and detected causal precursors are shown in Figs. 6a,b. MT rainfall has four causal precursors in OLR. A large region located over India and the Maritime Continent (OLR1, Fig. 6a) shows a negative causal link, while another region covering parts of the Himalayan plateau and extending toward the Arabian Peninsula shows a positive causal link (OLR2, Fig. 6a). A third region is found north of the Caspian Sea, over western Russia (OLR3) with a negative causal relationship with MT rainfall. Finally, a last region located over north/central Europe showing a negative causal relationship with MT rainfall is found (OLR4, Fig. 6a). OLR1 spatially overlaps with W1, the largest causal precursor in the vertical wind field, representing the summer branch of the ITCZ over the northern Indian Ocean and western Pacific Ocean (Fig. 6b, top panel). The positive correlation of W1 and negative correlation of OLR1 with MT rainfall indicate that ascending motions and associated high-level cloud formation (reducing OLR) are followed by enhanced rainfall over the MT region with a lag of 1 week. OLR2, OLR3 and OLR4 largely overlap with the regions H1 and L1 as well as the CGTI region identified in Fig. 4c, further supporting the importance of this mid-latitude wave pattern in modulating the rainfall over the MT region.

https://doi.org/10.5194/esd-2019-42
Preprint. Discussion started: 5 August 2019
© Author(s) 2019. CC BY 4.0 License.

Earth System Dynamics
Discussions
Open Access
EGU

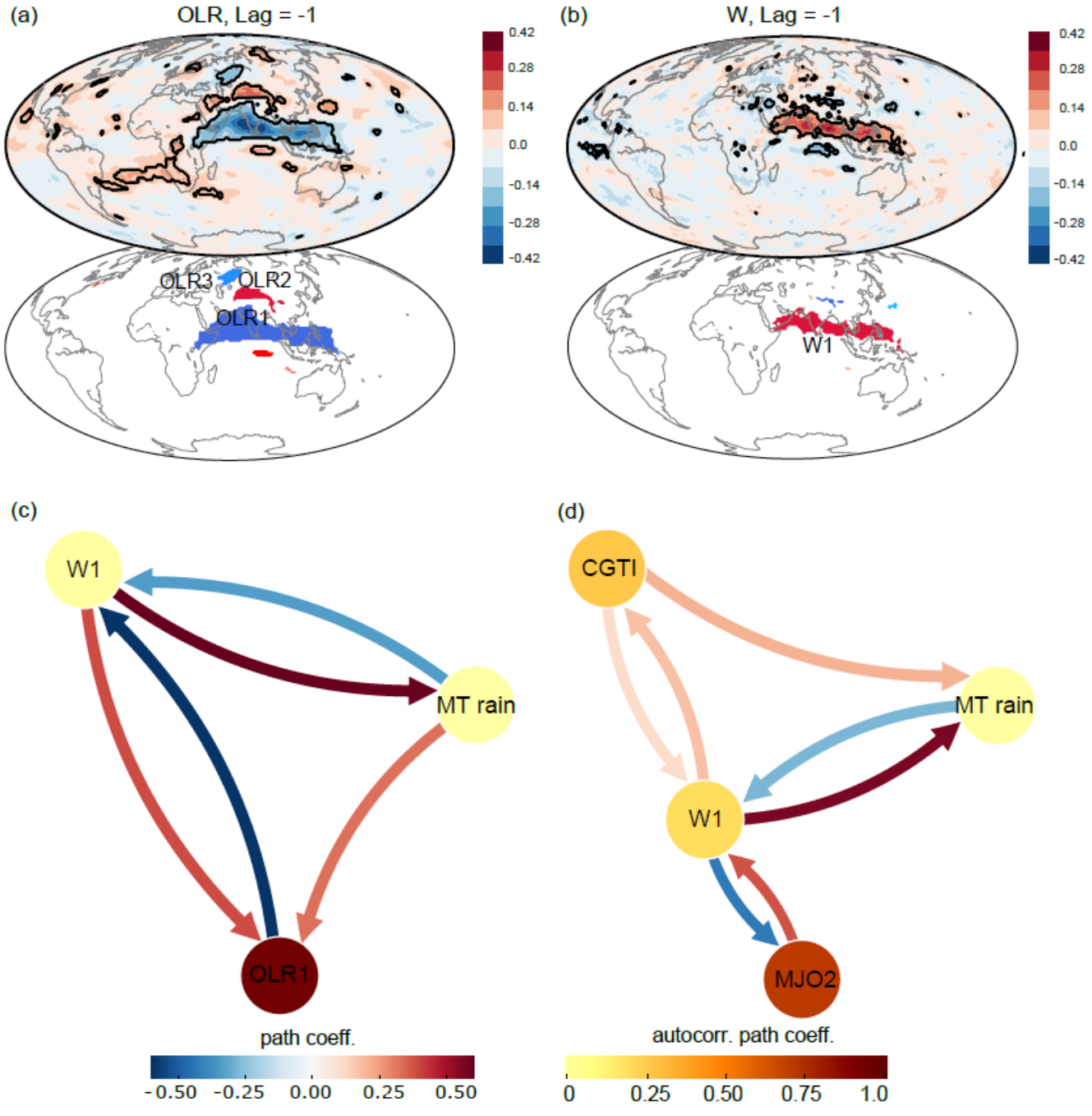

Figure 6. Tropical causal interactions of ISM. Panel (a) shows the correlation map of weekly MT rainfall with the global OLR field at 1-week lead time (top panel) and the causal precursors identified via RG-CPD (bottom panel) for the period 1979-2017. Panels (b): as for panel (a) but for the W field. Panels (c) and (d) show the CENs build with W1, OLR1 and MT rainfall and MT rainfall, W1, CGTI and

https://doi.org/10.5194/esd-2019-42
Preprint. Discussion started: 5 August 2019
© Author(s) 2019. CC BY 4.0 License.


MJO2, respectively. The strength of causal links expressed by the standardized regression path coefficients and autocorrelation path coefficients are shown. All links have a lag of 1 week. See the main text for discussion.

365

Figures 6c,d show two CENs constructed from the MT rainfall causal precursors in OLR and W (region OLR1 as defined in Fig. 6a and W1 as defined in Fig. 6b), and including CGTI and MT rainfall itself. Since the OLR and W fields are more noisy than Z200, we use only the two dominant causal precursors. Although the regions OLR1 and W1 show a large spatial overlap, they represent two different components of the ISM system. OLR is calculated at the top of the atmosphere and low OLR
370 values represent high clouds that reach the top of the troposphere. Thus, OLR is a proxy for deep convection and clouds. W is calculated at 500 hPa and W1 thus represents the ascending branch of the ISM circulation cell and nearby ITCZ. The CEN built with OLR1, W1 and the MT rainfall at weekly timescale (Fig. 6c) represents the internal dynamics of the monsoon cell. Enhanced vertical motions (W1) precede an increase in the MT rainfall by one week, while stronger MT rainfall leads to weaker ascending motions one week later. Meanwhile, more clouds (lower OLR1) are associated with enhanced W1 one week
375 later (thus enhancing the ISM circulation). Contrarily, enhanced rainfall shows a negative feedback on both OLR1 and W1: stronger MT rainfall leads to reduced vertical motions and clearer skies (lower W1 and higher OLR1, respectively). This CEN thus depicts a negative feedback intrinsic to the ISM internal variability: while enhanced ascending motions and thus strengthened ISM circulation lead to stronger MT rainfall, enhanced rainfall leads to weaker ISM circulation and in turn diminished MT rainfall. From a physical point of view, this can be explained via an increase of atmospheric static stability due
380 to latent heat release in the higher layers of the troposphere. This mechanism is shown in Fig. S9 (see SI), where we build a CEN with MT rainfall, sea level pressure (SLP) over the Bay of Bengal (SLP_BOB), temperature at 400hPa (Tp4_MT) and temperature at 600 hPa (Tp6_MT). The resulting causal links show that while a decrease in SLP over the Bay of Bengal is followed by an increase in MT rainfall and both Tp4_MT and Tp6_MT, an increase in Tp4_MT leads to a decrease in MT rainfall. The described mechanism is in agreement with what was proposed by Saha et al. (2012) and Krishnamurti and Bhalme
385 (1976).

Next, we test the causal relationships identified between MT rainfall and W1 when adding the CGTI and MJO variability to the CEN (Fig. 6d). MJO variability is expressed by the OMI PC2 index (here referred to as MJO2), the second EOF of OLR in the tropical belt (Kiladis et al., 2014). OMI PC2 corresponds to the RMM1 index, widely used in previous work on the relationship between the MJO and the ISM (Kiladis et al., 2014; Mishra et al., 2017; Pai et al., 2011). Positive RMM1 values
390 correspond to MJO phases 3-6 (also referred to as the active phases of MJO) and physically represent the presence of strong convection activity propagating eastward from the Indian Ocean towards the western Pacific. Several studies show that MT rainfall is enhanced during the active MJO phase (Anandh et al., 2018; Mishra et al., 2017; Pai et al., 2011). In this CEN, the links between the MT rainfall and W1 remain unaltered, while the CGTI shows a positive feedback with W1: an increase in the CGTI causes stronger ascending motions, while stronger ascending motion over the Indian region strengthens the CGTI.
395 The CGTI has a direct positive causal link to MT rainfall (Fig. 6d). Even though the direct link from MT rainfall to CGTI has

https://doi.org/10.5194/esd-2019-42
Preprint. Discussion started: 5 August 2019
© Author(s) 2019. CC BY 4.0 License.


now disappeared (likely because this link was already relatively weak in a simpler CEN configuration, see Fig. 3a), the link between the ISM circulation and the mid-latitudes remains via W1. Stronger ISM circulation (higher W1) leads to increased CGTI and vice versa as seen in Fig. 3, where higher CGTI leads to enhanced MT rainfall and vice versa. MJO2 displays a positive causal link with W1, meaning that OMI PC2 positive values lead to enhanced vertical motions with 1-week lead time and, as a consequence, enhanced MT rainfall with 2-week lead time. However, stronger W1 leads to decreased MJO2 (negative causal link from W1 to MJO2). Thus, MJO2 shows exactly the same causal relationships (but opposite signs) with W1 as shown for OLR1 in Fig. 6c, likely because the OMI index is also defined based upon OLR fields in the tropical belt and the OLR pattern shown by the second EOF of the OMI index largely overlaps with our OLR1 region (Kiladis et al., 2014).

3.4: Combining local, tropical and mid-latitude causal interactions

Finally, we bring together the findings obtained with CEN and RG-CPD throughout this study and summarize them in a single CEN to provide an overall picture and test the consistency of the results. We include the most important identified regions from both the tropics and the mid-latitudes together in a single CEN (Fig. 7). Specifically, this CEN is built with elements that come from both, the DW2005 and DW2007 hypotheses (Fig. 3) and from our RG-CPD analysis (Figs. 4 and 6). Our results show that the influence of both, the mid-latitude circulation (EOF2) and the North Atlantic (NAO), on the MT rainfall is mediated via the CGTI and is robust: the structure and the direction of the causal links are retained. The backward influence of the MT rainfall on the mid-latitude circulation is weaker and more complex, as shown in Fig. 6d. CGTI has both a direct causal link to MT rainfall and an indirect one via W1.

https://doi.org/10.5194/esd-2019-42
Preprint. Discussion started: 5 August 2019
© Author(s) 2019. CC BY 4.0 License.

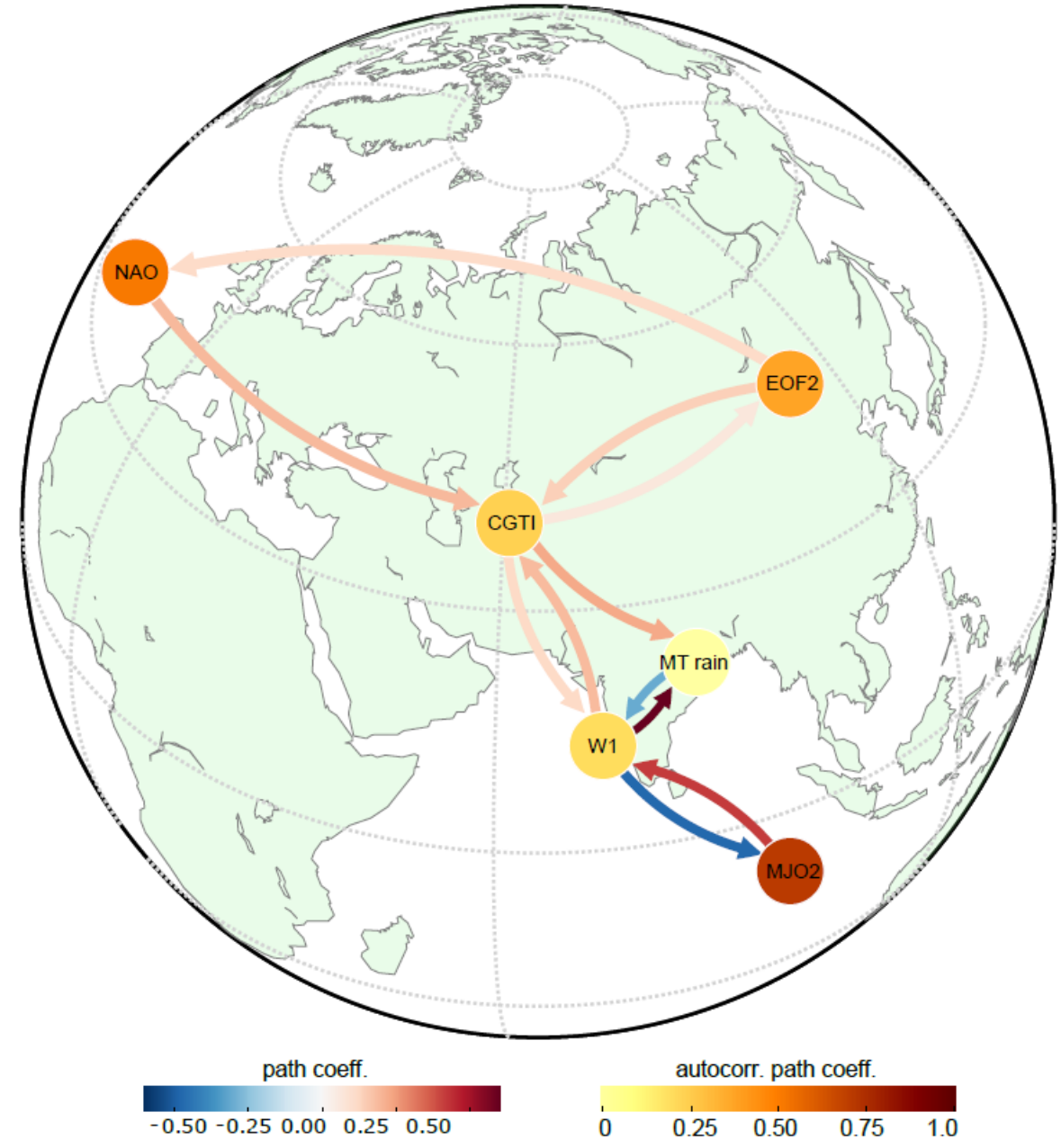

Figure 7. Combined mid-latitude and tropical causal interactions of ISM. CEN built with W1, MJO2, MT rainfall, NAO, CGTI and EOF2 for the period 1979-2017. The strength of causal links expressed by the standardized regression path coefficients and autocorrelation path coefficients are shown. All links have a lag of 1 week. See the main text for discussion.

https://doi.org/10.5194/esd-2019-42
Preprint. Discussion started: 5 August 2019
© Author(s) 2019. CC BY 4.0 License.

Earth System Dynamics Discussions

MT rainfall and W1 show a negative feedback, with increased W1 leading to enhanced MT rainfall but stronger MT rainfall leading to weaker W1. The MT rainfall is also influenced by MJO2 via W1 with a one-way connection. Suppressed or weakened ascending motions promote lower MJO2 one week after, thus promoting the switch toward MJO phases 7-8 and 1-2, also known as suppressed MJO phases. Suppressed MJO phases are in turn linked with the onset of break phases of the Indian monsoon (Pai et al., 2011).

To quantify the relative influence of tropical and mid-latitude teleconnections on MT rainfall, we report the causal effect (CE) strength of each link, which is given by the path coefficient in the CEN.W1 has the strongest causal effect on MT rainfall with $\beta_{W1\rightarrow MT} = 0.52$, implying that a one s.d. shift in W1 causes about a half s.d. change in MT rainfall after one week (under the previously mentioned conditions, see Methods section). The CGTI influences MT rainfall directly and indirectly via W1 and the total causal effect is given by $\beta_{CGTI\rightarrow MT} + \beta_{CGTI\rightarrow W1} \cdot \beta_{W1\rightarrow MT} = 0.24$, where $\beta_{CGTI\rightarrow MT} = 0.19$ and $\beta_{CGTI\rightarrow W1} = 0.10$ The causal effect of CGTI is thus roughly half as strong as that of the internal variability of the Indian monsoon system as represented here by W1. MJO2 has a causal effect on W1 of $\beta_{MJO2\rightarrow W1} = 0.35$ and is influenced by W1 with $\beta_{W1\rightarrow MJO2} = -0.39$. Thus, taking both W1 and MT as representatives of internal ISM dynamics, the effects of external drivers from both tropics and mid-latitudes on this internal dynamics are both of the order of half as strong as that of W1 on MT. Looking more specifically at the causal effect of MJO2 on MT rainfall mediated via W1, we find $\beta_{MJO2\rightarrow W1}*\beta_{W1\rightarrow MT} = 0.18$, i.e., the tropical driver effect on MT rainfall itself is similar in magnitude as that of CGTI as the key extratropical driver. The path coefficients for all the identified causal links are reported in Table S1 (see SI).

Moreover, we calculate the average causal effect (ACE) and average causal susceptibility (ACS) for each actor. While ACE gives a measure of the causal effect that each actor has on the rest of the network, ACS measures the sensitivity of each actor to perturbations entering in any other part of the network (Runge et al., 2015a). In this CEN, W1 has the highest ACE (~0.21) and both CGTI and MJO2 the second highest ACE (~0.07). MT rainfall and W1 show the strongest ACS (~0.1). ACE and ACS values for each actor are further summarized in Table S2, see SI. These values again stress the importance of both, ISM internal variability and CGTI, in mediating mid-latitude waves towards the ISM.

We performed the same analysis using the CPC-NCEP rainfall dataset over the period 1979-2016 (see SI, Figs. S10-S16) and find that our results are robust when using this different rainfall dataset. All causal links are reproduced with the same directions and only the magnitudes of the causal effects show minor changes.

4. Discussion and conclusions

In this study, we apply causal discovery algorithms to analyse the influence of global middle and upper tropospheric fields on the ISM rainfall and study the two-way causal links between the mid-latitude circulation and ISM rainfall. We perform a validation of both the monsoon-circumglobal teleconnection hypothesis proposed by DW2005 and the North Atlantic-monsoon connection proposed by DW2007 using causal discovery tools. We use RG-CPD to detect causal precursors from

https://doi.org/10.5194/esd-2019-42
Preprint. Discussion started: 5 August 2019
© Author(s) 2019. CC BY 4.0 License.


both mid-latitude and tropical regions and then apply CEN to assess the influence of different drivers of MT rainfall and their relative contribution to the MT rainfall sub-seasonal variability.

The new findings of this work can be summarized in two main aspects: first, we prove the DW2005 hypothesis from a causal point of view, showing that the hypothesized two-way link between the MT rainfall and the mid-latitude circulation is detected in a causal framework. Second, we quantify the relative importance of a) the mid-latitude circulation, b) the internal dynamics of the convection cell and c) the Madden-Julian Oscillation (MJO) on the ISM subseasonal variability (see Figure 7 and Table S1 in the SI). Moreover, we also show that the circumglobal teleconnection hypothesis by DW2005, initially defined at seasonal/monthly time scale, holds also at sub-seasonal (weekly) time scale and it can be unified with the hypothesis by DW2007, which analysed wave trains propagating from the North Atlantic toward the MT region at 2-week time scale. Thus, we argue that the CGTI region and the mid-latitude circulation are important for both the sub-seasonal and interannual variability of the MT rainfall.

Our causal analyses confirm the influence of the mid-latitude circulation on MT rainfall via the CGTI, as hypothesized by DW2005. We also confirm that MT rainfall forces the mid-latitude circulation via the CGTI but this link is weaker. Moreover, we use a causal precursor identification tool and find a wave train that emanates from the eastern Atlantic stretching towards India. This wave pattern is visible in geopotential height fields, temperature and precipitation anomalies, and acts on MT rainfall via the CGTI with a 1-2 week lead time, in agreement with the DW2007 hypothesis.

Our results show that RG-CPD can detect the well-known circulation features of the MT rainfall with 1-week lead time, without using any a priori theoretical or geographical constraint to select the causal precursors among all precursor regions demonstrating the efficacy of the presented method. Moreover, causal discovery tools can quantify the causal influence of tropical drivers versus extra-tropical influences and internal dynamics of the ISM sub-seasonal circulation dynamics.

Adding internal dynamics helps to further understand the mechanisms that underlie this mid-latitude-ISM relationship. Internal variability of the ISM system has the strongest effect on MT rainfall. The influence from the extratropics on MT rainfall, as mitigated by CGTI, is about half of the magnitude of that of internal dynamics, while the influence of MJO as the key tropical driver on MT rainfall is only slightly weaker (Fig. 7). However, when taking MT rainfall and vertical wind field over the Indian subcontinent together as two interdependent yet different facets of the ISM, we find that the general effect of tropical drivers on the system is slightly stronger than that of the extratropical drivers, while looking on the one hand on the effect of MJO on the circulation and on the other hand on the total effect of CGTI on MT rainfall via both, directed linkages and through a parallel influence on the vertical wind field over India.

The reported findings are in good agreement with the existing literature. It is well known that internal variability dominates ISM inter-annual variability (Goswami and Xavier, 2005). Our causal approach enables to quantify the relative importance of local internal dynamics, separate it from the influence of remote actors, and remove spurious factors. The negative feedback in the ISM internal variability, here represented by the opposite relationship between MT rainfall and W1 (see Figs. 6d and 7), further supports the hypothesis that the internal dynamics of the ISM itself provides a mechanism to switch from an active to a break phase. The physical mechanism can include both radiative effects (Krishnamurti and Bhalme, 1976) and

https://doi.org/10.5194/esd-2019-42
Preprint. Discussion started: 5 August 2019
© Author(s) 2019. CC BY 4.0 License.


local changes in static stability due to the latent heat release that follows convective precipitation (Saha et al., 2012). While strong upward motions precede strong MT rainfall, enhanced rainfall over the ITCZ region is known to lead the initiation of breaks by 7-10 days (Krishnan et al., 2000). Moreover, suppressed convection over the Bay of Bengal initiated over the tropical Indian Ocean and associated westward propagating Rossby waves bring break conditions over the monsoon trough (Krishnan et al., 2000).

Moreover, our results also support previous findings that suggest a link between the active MJO phases (3-6, corresponding to positive RMM1 values) and enhanced ascending motions over the MT region and adjacent Maritime Continent which in turn promote enhanced MT rainfall (Fig. 6d and 7) (Anandh et al., 2018; Mishra et al., 2017; Pai et al., 2011).

Our theory-guided causal effect network approach, i.e. creating CENs starting from physical hypotheses, enables us to: (1) test those hypotheses in a causal framework, removing the influence from spurious correlations, and (2) quantify the relative strength (i.e. causal effect) of different local and remote actors. With this approach, one can gain insight in which role each part of a complex system such as the ISM circulation plays in relation to the other components. However, domain knowledge is essential to be guided by known physical processes and associated timescales. By combining RG-CPD and CEN, one can test initial hypotheses and perform further more explorative causal analyses to identify new features. For example, in this study, we first identify our initial actors based on the literature. Then, we increase the pool of actors by searching for causal precursors using RG-CPD. Finally, we reconstruct a CEN that combines those findings and helps to put them into a broader context. This approach can be applied to both observational data (as done here) and climate model data to validate the underlying processes behind sub-seasonal variability, which might pave the way for improved forecasts.

The described identification and quantification of causal dependences is based on linear statistical models between the different considered variables quantified in terms of partial correlations. While such linear models can provide useful approximations of real-world climate processes, there could be cases in which they miss other existing linkages that are not described by linear functional relationships. In turn, extending the present analysis to a fully nonlinear treatment is straightforward but would come on the cost of much higher computational demands, which is why we have restricted ourselves in this work to the linear case. Nevertheless, accounting for possible nonlinearities may add further information on the inferred mechanisms and should therefore be undertaken in future research.

Our results indicate that, on weekly timescales, the strength of the influence from the mid-latitudes on MT rainfall itself is as large as that from the tropics (MJO) but about a factor two smaller than the ISM internal dynamics. However, the tropical (MJO) effect on the associated vertical wind speed over the MT region is larger than that of extratropical drivers on MT rainfall. Related to the confirmed relevance of extratropical drivers for ISM variability at weekly scales, we emphasise that there exists a substantial body of literature suggesting that the influence from the mid-latitudes is particularly important for extremes (Lau and Kim, 2011; Vellore et al., 2014, 2016). Future work should therefore aim to further disentangle the specific mechanisms that particularly act in the context of extremes.

https://doi.org/10.5194/esd-2019-42
Preprint. Discussion started: 5 August 2019
© Author(s) 2019. CC BY 4.0 License.

Earth System Dynamics Discussions

Acknowledgments

We thank ECMWF and NCEP for making the ERA-Interim and CPC data available. This work was supported by the German Federal Ministry of Education and Research (projects GOTHAM, Sacre-X and CoSy-CC^2). Code for the causal discovery algorithm is freely available as part of the Tigramite Python software package at https://github.com/jakobrunge/tigramite.

References

Anandh, P. C., Vissa, N. K. and Broderick, C.: Role of MJO in modulating rainfall characteristics observed over India in all seasons utilizing TRMM, Int. J. Climatol., 38(5), 2352–2373, doi:10.1002/joc.5339, 2018.

Bello, G. A., Angus, M., Pedemane, N., Harlalka, J. K., Semazzi, F. H. M., Kumar, V. and Samatova, N. F.: Response-Guided Community Detection: Application to Climate Index Discovery, in Machine Learning and Knowledge Discovery in Databases, pp. 736–751., 2015.

Benjamini, Y. and Hochberg, Y.: Controlling the False Discovery Rate: a Practical and Powerful Approach to Multiple Testing, J. R. Stat. Soc. Ser. B, 57(1), 289–300, doi:10.2307/2346101, 1995.

Benjamini, Y. and Yekutieli, D.: The control of the false discovery rate in multiple testing under dependency, Ann. Stat., 29(4), 1165–1188, doi:10.1214/aos/1013699998, 2001.

Chattopadhyay, R., Goswami, B. N., Sahai, A. K. and Fraedrich, K.: Role of stratiform rainfall in modifying the northward propagation of monsoon intraseasonal oscillation, J. Geophys. Res., 114, D19114, doi:10.1029/2009JD011869, 2009.

Chen, M., Shi, W., Xie, P., Silva, V. B. S., Kousky, V. E., Higgins, R. W. and Janowiak, J. E.: Assessing objective techniques for gauge-based analyses of global daily precipitation, J. Geophys. Res. Atmos., 113(4), 1–13, doi:10.1029/2007JD009132, 2008.

Choudhury, A. D. and Krishnan, R.: Dynamical Response of the South Asian Monsoon Trough to Latent Heating from Stratiform and Convective Precipitation, J. Atmos. Sci., 68(6), 1347–1363, doi:10.1175/2011JAS3705.1, 2011.

Dee, D. P., Uppala, S. M., Simmons, a. J., Berrisford, P., Poli, P., Kobayashi, S., Andrae, U., Balmaseda, M. a., Balsamo, G., Bauer, P., Bechtold, P., Beljaars, a. C. M., van de Berg, L., Bidlot, J., Bormann, N., Delsol, C., Dragani, R., Fuentes, M., Geer, a. J., Haimberger, L., Healy, S. B., Hersbach, H., Hólm, E. V., Isaksen, L., Kållberg, P., Köhler, M., Matricardi, M., Mcnally, a. P., Monge-Sanz, B. M., Morcrette, J. J., Park, B. K., Peubey, C., de Rosnay, P., Tavolato, C., Thépaut, J. N. and Vitart, F.: The ERA-Interim reanalysis: Configuration and performance of the data assimilation system, Q. J. R. Meteorol. Soc., 137(656), 553–597, doi:10.1002/qj.828, 2011.

Ding, Q. and Wang, B.: Circumglobal teleconnection in the Northern Hemisphere summer, J. Clim., 18(17), 3483–3505, doi:10.1175/JCLI3473.1, 2005.

Ding, Q. and Wang, B.: Intraseasonal teleconnection between the summer Eurasian wave train and the Indian Monsoon, J. Clim., 20(15), 3751–3767, doi:10.1175/JCLI4221.1, 2007.

https://doi.org/10.5194/esd-2019-42
Preprint. Discussion started: 5 August 2019
© Author(s) 2019. CC BY 4.0 License.

Gadgil, S. and Joseph, P. V: On breaks of the Indian monsoon, Proc. Indian Acad. Sci. (Earth Planet. Sci.), 112(4), 529–558, doi:https://doi.org/10.1007/BF02709778, 2003.

Goswami, B. N. and Xavier, P. K.: Dynamics of "internal" interannual variability of the Indian summer monsoon in a GCM, J. Geophys. Res., 110, D24104, doi:10.1029/2005JD006042, 2005.

Hannachi, a., Jolliffe, I. T. and Stephenson, D. B.: Empirical orthogonal functions and related techniques in atmospheric science: A review, , 713(November 2006), 697–713, doi:10.1002/joc, 2007.

Houze Jr, R. A., McMurdie, L. A., Rasmussen, K. L., Kumar, A. and Chaplin, M. M.: Multiscale Aspects of the Storm Producing the June 2013 Flooding in Uttarakhand, India, Mon. Weather Rev., 145, 4447–4466, doi:10.1175/mwr-d-17-0004.1, 2017.

Kiladis, G. N., Dias, J., Straub, K. H., Wheeler, M. C., Tulich, S. N., Kikuchi, K., Weickmann, K. M. and Ventrice, M. J.: A Comparison of OLR and Circulation-Based Indices for Tracking the MJO, Mon. Weather Rev., 142, 1697–1715, doi:10.1175/MWR-D-13-00301.1, 2014.

Kretschmer, M., Coumou, D., Donges, J. F., Runge, J. and Donges, J. F.: Using Causal Effect Networks to analyze different Arctic drivers of mid-latitude winter circulation, J. Clim., 29, 4069–4081, doi:10.1175/JCLI-D-15-0654.1, 2016.

Kretschmer, M., Runge, J. and Coumou, D.: Early prediction of extreme stratospheric polar vortex states based on causal precursors, Geophys. Res. Lett., 44(16), 1–9, doi:10.1002/2017GL074696, 2017.

Kripalani, R. H. Ã., Kulkarni, A. and Singh, S. V: Association of the Indian Summer Monsoon with the Northern Hemisphere Mid-Latitude Circulation, Int. J. Climatol., 17, 1055–1067, doi:https://doi.org/10.1002/(SICI)1097-0088(199708)17:10<1055::AID-JOC180>3.0.CO;2-3, 1997.

Krishnamurti, T. N. and Bhalme, H. H.: Oscillations of a monsoon system Part I: Observational apects, J. Atmos. Sci., 33, 1937–1954, doi:10.1175/1520-0469(1976)033<1937:OOAMSP>2.0.CO;2, 1976.

Krishnamurti, T. N. and Surgi, N.: Observational aspects of the summer monsoon, in Monsoon Meteorology, edited by C.-P. Chang and T. N. Krishnamurti, pp. 3–25, Oxford University Press., 1987.

Krishnan, R., Zhang, C. and Sugi, M.: Dynamics of Breaks in the Indian Summer Monsoon, J. Atmos. Sci., 57(1969), 1354–1372, 2000.

Krishnan, R., Kumar, V., Sugi, M. and Yoshimura, J.: Internal Feedbacks from Monsoon – Midlatitude Interactions during Droughts in the Indian Summer Monsoon, J. Atmos. Sci., 66, 553–578, doi:10.1175/2008JAS2723.1, 2009.

Lau, W. K. M. and Kim, K.-M.: The 2010 Pakistan Flood and Russian Heat Wave : Teleconnection of Hydrometeorological Extremes, J. Hydrometeorol., 13, 392–403, doi:10.1175/JHM-D-11-016.1, 2011.

Levermann, A., Schewe, J., Petoukhov, V. and Held, H.: Basic mechanism for abrupt monsoon transitions Anders, Proc. Natl. Acad. Sci., 106(49), 20572–20577, doi:10.1073/pnas.0901414106, 2009.

Mishra, S. K., Sahany, S. and Salunke, P.: Linkages between MJO and summer monsoon rainfall over India and surrounding region, Meteorol. Atmos. Phys., 129(3), 283–296, doi:10.1007/s00703-016-0470-0, 2017.

North, G. R., Bell, T. L., Cahalan, R. F. and Moeng, F. J.: Sampling Errors in the Estimation of empirical Orthogonal Functions,

https://doi.org/10.5194/esd-2019-42
Preprint. Discussion started: 5 August 2019
© Author(s) 2019. CC BY 4.0 License.

Mon. Weather Rev., 110, 699–706, doi:https://doi.org/10.1175/1520-0493(1982)110<0699:SEITEO>2.0.CO;2, 1982.

Pai, D. S., Bhate, J., Sreejith, O. P. and Hatwar, H. R.: Impact of MJO on the intraseasonal variation of summer monsoon rainfall over India, Clim. Dyn., 36(1), 41–55, doi:10.1007/s00382-009-0634-4, 2011.

Pai, D. S., Latha, D. S. P., Badwaik, S. M. R. and Rajeevan, M.: Analysis of the daily rainfall events over India using a new long period (1901–2010) high resolution (0.25° × 0.25°) gridded rainfall data set, Clim. Dyn., 45, 755–776, doi:10.1007/s00382-014-2307-1, 2015.

Pathak, A., Ghosh, S., Kumar, P. and Murtugudde, R.: Role of Oceanic and Terrestrial Atmospheric Moisture Sources in Intraseasonal Variability of Indian Summer Monsoon Rainfall, Sci. Rep., 7(1), 12729, doi:10.1038/s41598-017-13115-7, 2017.

Rao, Y. P.: Southwest monsoon, METEOROLOG., Meteorological Monograph: Synoptic Meteorology., 1976.

Runge, J.: Causal network reconstruction from time series : From theoretical assumptions to practical estimation, Chaos, 28, 075310, doi:10.1063/1.5025050, 2018.

Runge, J., Heitzig, J., Marwan, N. and Kurths, J.: Quantifying causal coupling strength: A lag-specific measure for multivariate time series related to transfer entropy, Phys. Rev. E, 86(6), 061121, doi:10.1103/PhysRevE.86.061121, 2012.

Runge, J., Petoukhov, V. and Kurths, J.: Quantifying the strength and delay of climatic interactions: The ambiguities of cross correlation and a novel measure based on graphical models, J. Clim., 27(2), 720–739, doi:10.1175/JCLI-D-13-00159.1, 2014.

Runge, J., Petoukhov, V., Donges, J. F., Hlinka, J., Jajcay, N., Vejmelka, M., Hartman, D., Marwan, N., Paluš, M. and Kurths, J.: Identifying causal gateways and mediators in complex spatio-temporal systems, Nat. Commun., 6, 9502, doi:10.1038/ncomms9502, 2015a.

Runge, J., Donner, R. V. and Kurths, J.: Optimal model-free prediction from multivariate time series, Phys. Rev. E - Stat. Nonlinear, Soft Matter Phys., 91(5), 052909, doi:10.1103/PhysRevE.91.052909, 2015b.

Runge, J., Sejdinovic, D. and Flaxman, S.: Detecting causal associations in large nonlinear time series datasets, , doi:arXiv:1702.07007, 2017.

Saeed, S., Müller, W. A., Hagemann, S., Jacob, D., Mujumdar, M. and Krishnan, R.: Precipitation variability over the South Asian monsoon heat low and associated teleconnections, Geophys. Res. Lett., 38, L08702, doi:10.1029/2011GL046984, 2011.

Saha, S. K., Halder, S., Suryachandra Rao, A. and Goswami, B. N.: Modulation of ISOs by land-atmosphere feedback and contribution to the interannual variability of Indian summer monsoon, J. Geophys. Res. Atmos., 117(13), 1–14, doi:10.1029/2011JD017291, 2012.

Schleussner, C. F., Runge, J., Lehmann, J. and Levermann, a.: The role of the North Atlantic overturning and deep ocean for multi-decadal global-mean-temperature variability, Earth Syst. Dyn., 5(1), 103–115, doi:10.5194/esd-5-103-2014, 2014.

Shige, S., Nakano, Y. and Yamamoto, M. K.: Role of Orography , Diurnal Cycle , and Intraseasonal Oscillation in Summer Monsoon Rainfall over the Western Ghats and Myanmar Coast, J. Clim., 30, 9365–9381, doi:10.1175/JCLI-D-16-0858.1, 2017.

Spirtes, P., Glymour, C. and Scheines, R.: Causation, prediction, and search, Boston: The MIT Press., 2000.

Vellore, R. K., Krishnan, R., Pendharkar, J., Choudhury, A. D. and Sabin, T. P.: On the anomalous precipitation enhancement

https://doi.org/10.5194/esd-2019-42
Preprint. Discussion started: 5 August 2019
© Author(s) 2019. CC BY 4.0 License.


over the Himalayan foothills during monsoon breaks, Clim. Dyn., 43(7–8), 2009–2031, doi:10.1007/s00382-013-2024-1, 2014.

Vellore, R. K., Kaplan, M. L., John, R. K., Sabade, S., Deshpande, N. and Singh, B. B.: Monsoon - extratropical circulation interactions in Himalayan extreme rainfall, Clim. Dyn., 46(11), 3517–3546, doi:10.1007/s00382-015-2784-x, 2016.

Wang, B., Webster, P., Kikuchi, K., Yasunari, T. and Qi, Y.: Boreal summer quasi-monthly oscillation in the global tropics, Clim. Dyn., 16, 661–675, doi:10.1007/s00382-006-0163-3, 2006.

Wheeler, M. C. and Hendon, H. H.: An All-Season Real-Time Multivariate MJO Index: Development of an Index for Monitoring and Prediction, Mon. Weather Rev., 132(8), 1917–1932, doi:10.1175/1520-0493(2004)132<1917:AARMMI>2.0.CO;2, 2004.

Willink, D., Khan, V. and Donner, R. V.: Improved one-month lead-time forecasting of the SPI over Russia with pressure covariates based on the SL–AV model, Q. J. R. Meteorol. Soc., 143(707), 2636–2649, doi:10.1002/qj.3114, 2017.

Yanai, M. and Wu, G.: Effects of the tibetan plateau, in The Asian Monsoon, pp. 513–549, Springer., 2006.

Zhang, C.: Madden-Julian Oscillation, Rev. Geophys., 43, RG2003, doi:10.1029/2004RG000158, 2005.